Leveraging Analogues for CO_2 Core Flood Experiments: Enhancing Reservoir Simulation Inputs

Egil Boye Petersen[1,*], *Reza Askarinezhad*[2], *Arild Lohne*[2] ,*John C. Zuta*[2], *and Ronald Sørlie*[1]

[1]AkerBP, Norway
[2]NORCE Norwegian Research Centre, Subsurface Flow Laboratory, Norway – Stavanger.

Abstract. Carbon capture and storage (CCS) initiatives rely on robust CO_2 core flood experiments to clarify transport and trapping mechanisms within geological formations. However, a paucity of reservoir-condition experimental data often hampers the direct application of field core results for reservoir simulation. This paper emphasizes the critical need for analogues in CO_2 core flood experiments, especially in areas where such data remain sparse. Steady-state drainage relative permeability measurements were conducted at representative reservoir conditions, using equilibrated CO_2 and synthetic formation water (SFW) on reservoir core samples. These measurements were complemented by 1D X-ray scanning of average water saturations and differential pressures, followed by history matching (HM) to validate experimental observations. X-ray diffraction (XRD) analyses revealed that calcite concentrations ranged from 5% to 30% in the studied reservoir rocks. An automatic history-matching approach, employing a specialized core flood simulator, was utilized to estimate key parameters. Compositional simulation further assessed the impact of differential pressure, carbonate dissolution, and CO_2 dissolution on phase-property variations. Minor geochemical effects were observed, attributable to the relatively high brine salinity and low differential pressures. Consequently, chemical reactions were deemed negligible for history matching under the conditions studied. Further validation included the integration of capillary pressure data measured via Mercury Intrusion Capillary Pressure (MICP). The MICP-derived capillary pressures correlated closely with the estimated values across the experimentally relevant saturation range, indicating that any potential wettability shifts were either minor or negligible. This consistency supports MICP-based capillary pressure as a sound proxy for the CO_2/brine system under reservoir conditions. From these analogue-driven experimental outcomes, a comprehensive SCAL model—including an uncertainty range—was developed and used to inform subsequent reservoir simulations. This model is essential for refining our understanding of CO_2 storage potential on the Norwegian Continental Shelf (NCS), and the results were benchmarked against existing data from the Northern Lights project. By highlighting the advantages of analogues, this study encourages their broader use in CO_2 core flood research, with the aim of improving CO_2 storage strategies and enhancing the effectiveness of reservoir simulations.

1 Introduction

Carbon Capture and Storage (CCS) is recognised as a cornerstone of every credible net-zero pathway. Among the geological options, saline aquifers dominate global storage capacity: they are widespread, often lie close to major emission hubs, and provide four complementary trapping mechanisms—structural, residual, solubility and mineral—that confer increasing security with time [1-4].

Designing and risk assessing an aquifer storage project, however, demands high quality special core analysis (SCAL) data measured at representative reservoir pressure, temperature and brine chemistry. Supercritical CO_2 alters interfacial tension, wettability and mineral equilibria; therefore k_r, Pc and residual saturation functions measured with ambient N_2/brine analogues can misrepresent CO_2 plume migration and trapping efficiency [5]. Because such high-fidelity data are scarce and scattered, an industry initiative is under way to build a contextualised digital SCAL repository [6], yet most projects must still assemble their own analogue mosaics.

Poseidon is a salt-cored anticline in the Norwegian-Danish Basin (blocks 10/7–10/9). Phase 1 plans to inject about 150 Mt CO_2 over 25 years through four vertical wells placed in two sandstone formations: the Upper Triassic Skagerrak and the Lower Jurassic Gassum formations. Both units have porosities above 20%. The only well on the structure, 10/8-1 (drilled in 1970–71), was not cored in these intervals, so no reservoir-condition plugs are available for SCAL

To obtain representative core material, we used the Ivar Aasen field as an analogue. The Ivar Aasen Field was selected as an analogue for Poseidon due to stratigraphic, depositional, and diagenetic similarities. Both fields contain Triassic–Early Jurassic continental sandstones of the Skagerrak Formation and Statfjord Group (Gassum Fm. in Poseidon), deposited by braided rivers and floodplains across the Utsira High and southern North *Sea. Comparable burial depths (~2500 m) suggest similar*

* Corresponding author: egil.boye.petersen@akerbp.com

compaction and cementation histories, supporting analogue suitability.

Seal Peel samples from Ivar Aasen cores, with permeabilities from 100 mD to 1 D, were chosen to represent the expected injection flow units at Poseidon, avoiding low-quality intervals. The Ivar Aasen dataset offers extensive, high-quality core coverage from multiple wells targeting the Skagerrak Fm. and thus provided optimal material for our CO_2/brine core flood program.

Analogue evaluation included QEMSCAN analysis of 29 drill cutting samples from well 10/8-1, alongside wireline logs and lithological descriptions. Core and log data from Norwegian, Danish, and onshore wells were also considered, but Ivar Aasen offered the best combination of data quality and geological match. As operator of PL001 since 2007, with significant drilling and production experience from Ivar Aasen since 2016, we have developed a robust understanding of these formations' reservoir properties. Cores from an upcoming Poseidon appraisal well will be tested later, but they were not available for this study.

To bridge the gap, we construct a **multiple analogue database** centred on **Ivar Aasen** core plugs, chosen for their similar mineralogy, permeability range, and Jurassic age. The complete analogue suite comprises

- Unsteady-state (USS) imbibition and steady-state (SS) primary drainage scCO_2/brine floods on Ivar Aasen plugs at reservoir P–T,
- Hg-air MICP on the same plugs, converted to CO_2/brine Pc,
- SS primary drainage and USS imbibition N_2/brine floods that extend the permeability window, and
- Classical centrifuge and porous-plate tests from neighbouring North-Sea sandstones.

All SS experiments are interpreted with an automatic LET-based history matching engine (IORCoreSim) that corrects for capillary-end effects and quantifies parameter uncertainty. Compositional and geochemical simulations confirm that, under Poseidon salinity and stress, calcite dissolution has negligible impact on k_r–Pc over core-flood timescales. The merged analogue suite is distilled into log-linear $\mathbf{S_{wir}}$**–k** and Lands-type $\mathbf{S_{gt}}$**–**$\mathbf{S_{wir}}$ endpoint relations and three coupled k_r–Pc families—optimistic, base and pessimistic—that envelope the full data scatter. These curves are grid-scaled and deployed in Poseidon's first dynamic reservoir model, demonstrating a transferable analogue-driven workflow for CO_2 storage projects that lack in-situ core material.

2 SCAL Analysis Framework

The Special Core Analysis (SCAL) framework for CO_2 storage in aquifers focuses on measuring and estimating key flow parameters that are critical for understanding CO_2 injection behaviour and long-term containment. Two essential components of a CO_2-SCAL program for saline aquifers are steady-state (SS) CO_2/brine drainage relative permeability experiments and unsteady-state (USS) trapped-gas measurements. Given the potential for geochemical reactivity, and subsequently alteration of fluid and rock properties under reservoir conditions in the presence of CO_2, it is strongly recommended that these experiments be conducted at realistic pressure and temperature conditions. This ensures that the effects of CO_2–brine–rock interactions are accurately captured in relative permeability and capillary pressure data. Capillary pressure can either be derived through history matching of steady-state flooding experiments or/and measured independently using dedicated laboratory techniques.

Before conducting the relative permeability and capillary pressure measurements on the plugs, proper plugs selection, plugs cleaning & preparation, and initial measurements are to be performed.

In addition to experimental workflow, proper interpretation of the obtained results, especially the SS data is crucial; this is primarily to correct for the inevitably existing experimental artefacts, the capillary end effects. This is very important during a drainage cycle under strongly water-wet condition. Through a proper history matching of the SS results one can both correct for end effects and obtain the capillary pressure functions. In this work, the history matching was performed using an automatic method implemented in NORCE's in-house simulator, the *IORCoreSim*.

2.1. Experimental Workflow

In this study, the experiments were conducted on reservoir core plugs from Ivar Aasen. The initial selection of core plugs was based on 2D CT-scan images to ensure both homogeneity and representativeness, while also capturing a good spread across the targeted permeability ranges (a broad permeability range of approximately 10 to 1000 millidarcies (mD).

All core plugs underwent an initial cleaning by flooding with synthetic formation water. This was followed solvent flooding both at ambient and 60°C. After cleaning, methanol permeability (K_{MeOH}) was measured. The plugs were then saturated with synthetic formation water (SFW) through miscible displacement after which absolute permeability to SFW (k_w) was measured. Finally, pore volume (Vp) was estimated using Mohr's titration method and remeasured at the end of the program.

Following the establishment of irreducible water saturation (S_{wir}) using the porous plate method on each core plug, the cores underwent the USS experiments for trapped gas measurements. After that the cores were cleaned and re-saturated again with equilibrated brine before the SS primary drainage experiments were performed.

The unsteady-state (USS) imbibition and steady-state (SS) drainage experiments were conducted on both single core plugs and composite cores (comprising two stacked plugs). USS experiments consisted of low-rate water injection (imbibition cycle) followed by incremental rate steps, aimed at determining the residual trapped gas saturation. SS experiments involved varying the fractional flow from 100% water to 100% gas (primary drainage cycle), with rate bumps introduced toward the end of each test. The unsteady-state (USS) experiments (for trapped gas measurements) were performed in upward direction whereas, steady-state (SS) drainage experiments were performed downwards to secure gravity stable flow in both flow processes. The reservoir conditions during the experiments were: Pore pressure (Ppore) = 193 bar, net confining pressure (NCP)=103 bar, and temperature (T)= 69°C. Thus, CO_2 was injected equilibrated with SFW at these test conditions.

Throughout the USS and SS experiments, differential pressure across the core, fluid production, and one-dimensional in-situ water saturation measurements (ISSM) along the core length using X-ray were continuously recorded. For the establishment of irreducible water saturation using the porous plate method at ambient conditions, water production was recorded over time.

The synthetic formation water used in the study is a high salinity (~250k ppm) brine with NaCl, NaI (as dopant), CaCl2, and MgCl2 content of 88k, 50k, 71k, and 7k ppm, respectively. XRD analysis for rock mineralogy: The XRD analysis reveals a quartz-dominated mineralogy (55.0%), but with a significant presence of carbonates—particularly dolomite (17.9%) and calcite (2.6%)—which together contribute to a total carbonate content of 22.5%. This notable carbonate fraction implies potential for geochemical reactivity. End-trims of the plugs were used for ambient capillary pressure measurements MICP and helium porosity determination.

2.2 History matching CO_2/Brine SS experiments

Steady-state primary drainage flooding experiments exhibit strong capillary end effects reflecting strong water wet nature of the core material. This necessitates correction of the obtained relative permeability data for this artefact before being use in developing SCAL models.

In all simulations, relative permeability and capillary pressure were represented using the LET [7,8] and Skjæveland functions [9], respectively. The use of J-scaling allows better representations of individual plug capillary pressure in composite cores.

$$k_{rj} = k_{rej} \cdot \frac{s_{jn}^{L_j}}{s_{jn}^{L_j} + E_j(1-s_{jn})^{T_j}}, \quad (1)$$

$$S_{jn} = \frac{S_j - S_{jr}}{1 - S_{wr} - S_{gr}},\ j = w, g. \quad (2)$$

$$J_{cgw} = \frac{C_L}{(S_w - S_L)^{EL}} - \frac{C_R}{(S_R - S_w)^{ER}} + C_0 \quad (3)$$

$$P_{cgw} = IFT_{gw} \cdot J_{gw} \sqrt{\phi/k} \quad (4)$$

The matching was based on measured differential pressures, average saturation during the steady-state drainage process and saturation profiles at the end of each drainage fraction, provided by 1-D X-ray scanning.

Single-component phase simulations (immiscible system) were carried out for all cores. Additionally, for some cores, history matching was repeated using compositional simulations of CO_2 + brine, including explicit representation of all ions in the brine. Geochemical reactions were not incorporated in history matching due to long simulation times; however, a forward test simulation was conducted using derived properties for one core plug.

For the composite cores, which exhibited clear saturation profile discontinuities between the two stacked plugs, history matching was repeated considering the discontinuity as a high-permeability zone, with its permeability estimated as one of the history-matching parameters. Further history matching was performed considering permeability differences between the plugs comprising each composite core but still using a single set of relative permeability and capillary pressure functions for the entire composite core.

CO_2 and brine properties – In the simulations with *IORCoreSim*, CO_2 in brine is computed with the models from Duan et al [10,11]. H_2O in the CO_2 gas phase and the gas density are computed with the Peng Robinson equation of state (PR EOS). Estimated properties at reservoir conditions are given in Table 1. that the brine viscosity and density are increased.

Table 1 CO_2 and brine properties at reservoir conditions.

Gas phase	ρ_g, **g/ml**	μ_g, **cp**
CO_2 + Brine	0.622	0.0483
Pure CO_2*	0.651	0.051
Water phase	ρ_w, **g/ml**	μ_w, **cp**
Brine + CO_2	1.161	0.695
Pure brine**	1.144	0.646

* Pure CO_2 properties obtained from NIST Chemistry WebBook.

** From literature data for individual salts[12] using mass-based weighting for density and mol-based weighting for viscosity.

The HMs were repeated and this time instead of including capillary pressure in the HM, the measured data from MICP measurements were used. This was to examine both the quality of the matching and compare the obtained relative permeability function with previous cases in which both relative permeability and capillary pressure included in the history matching.

3 Experimental and simulation Results

This section presents selected experimental results from steady-state core flooding tests, interpreted through detailed history matching using the *IORCoreSim*. For the section 3.1 and 3.2 results of primary drainage SS experiment on a single plug are elaborated. The analysis investigates multiple scenarios, including the treatment of CO_2 and brine as immiscible but at-equilibrium fluids, the influence of brine composition, the effects of discontinuities in composite core setups, and the impact of permeability contrasts between the constituent plugs. Furthermore, preliminary assessments of geochemical interactions are incorporated to explore their influence on the obtained relative permeability and capillary pressure curves. Furthermore, in section 3.3. effect of discontinuity between the plugs in a composite core during primary drainage SS experiment is elaborated by defining various scenarios.

3.1 Capillary end-effects

Differential pressure, production data, and in-situ saturation profiles (Figure 1a and Figure 1b) along the single-plug (with length, L=7.18 cm, porosity, ϕ=0.21, and absolute water permeability, k_w=1019 mD) were history matched by adjusting parameters in the relative permeability and capillary pressure functions. As shown in Figure 2, the data points represent experimental measurements, while the solid lines illustrate the relative permeability curves corrected through history matching. A comparison of these curves, along with the saturation profiles presented in Figure 1a reveals that a significant portion of the experimental saturation range is influenced by pronounced capillary end-effects. These effects lead to underestimation of both water and gas relative permeabilities in the uncorrected experimental data.

3.2 Compositional and Geochemical effects

The history matching is repeated with compositional simulations of CO_2 + brine, including explicit representation of all ions in the brine. The coupling to geochemical reactions is not included in the history matching due to long simulation times, but a forward test simulation with derived properties was run at the end.

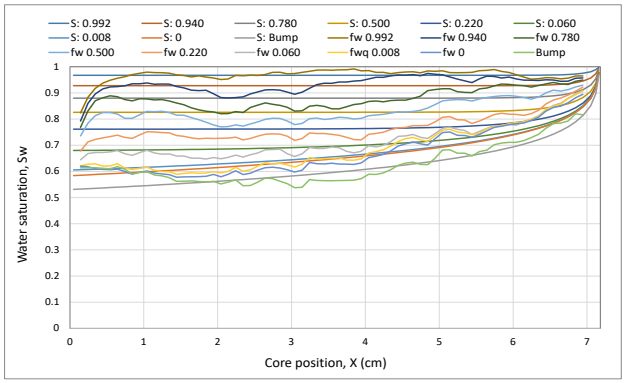

Figure 1a Experimental and simulated saturation profiles. From matching using single component phases. Fractional flow of water (f_w) is indicated in the legend, S: and f_w: indicate simulated and experimental data, respectively.

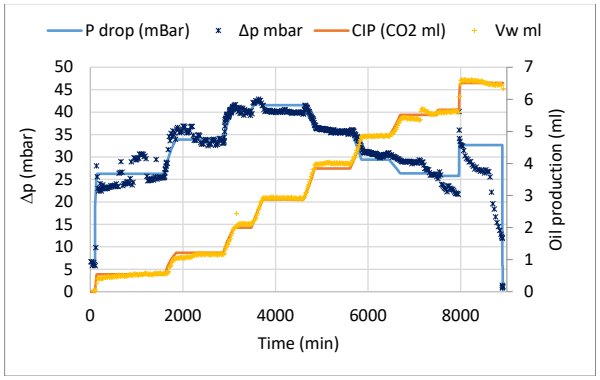

Figure 1b Simulated and experimental differential pressure, and water production.

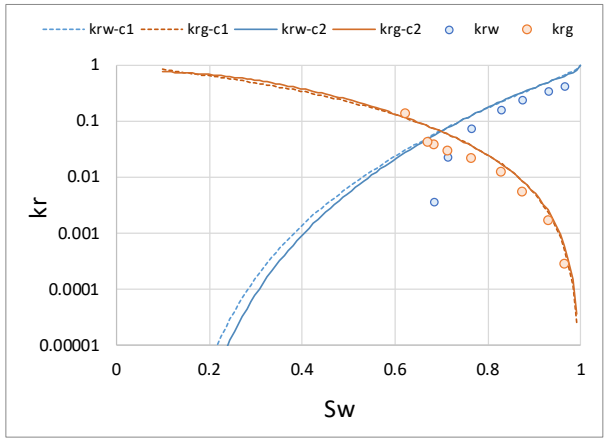

Figure 2 Relative permeability history matched SS experiment, single-component HM: c1 and Compositional HM: c2.

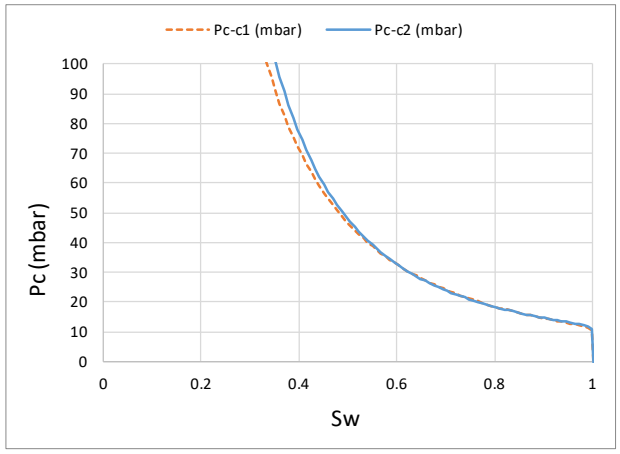

Figure 3 Capillary pressure history matched SS experiment, single-component HM: c1 and Compositional HM: c2.

As can be observed from Figure 2 and Figure 3, the estimated relative permeability and capillary pressure functions are practically the same as obtained with the immiscible two-phase (single-component) system except for the low water saturation range in which up to 10% increased/reduced estimated CO_2/Water relative permeabilities respectively. The resulting match of the differential pressure, production, and saturation profiles were close to experimental data shown in Figure 1 with some minor deviations.

Geochemical simulation - A forward simulation including geochemistry was run on a selected case. In this

simulation same relative permeability and capillary pressure functions as from the compositional HM were used. Only one mineral was considered here, the Calcite, which has relative fast dissolution/precipitation kinetic rates compared to other species at the experimental time scales.

The dissolution of CO_2 in the brine results in aqueous carbonate species (represented by $HCO3^-$) and decreased pH (i.e. increased H^+).

$$CO_2 + H_2O = H^+ + HCO_3^- \quad (5)$$

The low pH results in dissolution of calcite from the rock; this will result in increase in Ca^{++} and pH in the brine.

The observed increases in Ca^{++} and pH are small due to the initial high Ca^{++} content, in the brine, and will only result in minor changes in form of reduced solubility of CO_2 in the brine and small increments in the water-phase viscosity (0.695 -> 0.698 cp) and density (1.161 -> 1.162 g/ml), Figure 4.

Due to the minor effects observed on fluid properties in the present case, geochemical reactions can safely be ignored in the history matching simulations.

Note that dissolution of all carbonates in a core may have significant impact on the core permeability. The permeability may increase or be drastically reduced due to destabilisation of fines and clay particles. No such effects were included here. Also, other slower reactions involving dissolution of silicate and clay precipitation can affect the experiment.

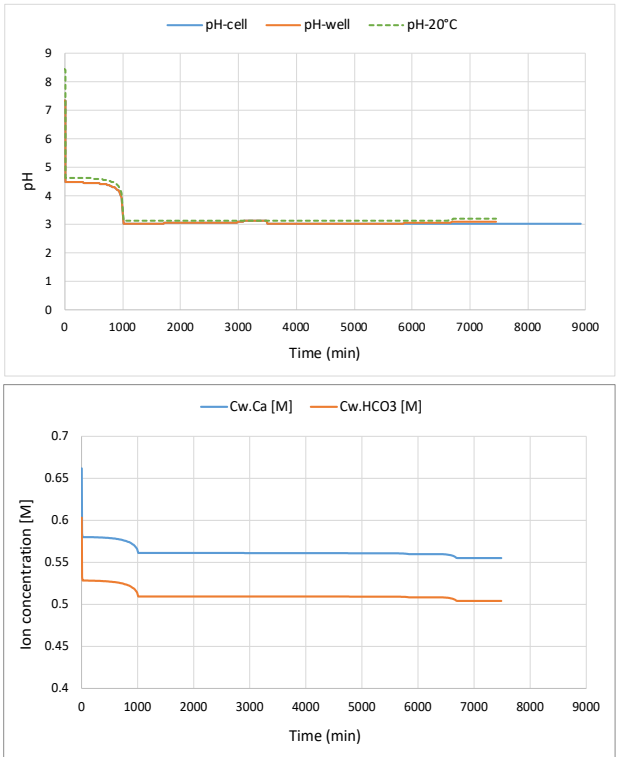

Figure 4 Simulated effluent pH (upper figure) and selected ion concentrations (Ca^{++} and $HCO3^-$) (bottom figure) with geochemical model activated. The 'pH-cell' is the outlet boundary cell, while 'pH-well' pH is computed for the well stream, both at reservoir temperature 69°C. 'pH-20°C' represents the well stream pH at 20 °C, assuming the same composition of the produced water phase (i.e., no boiling of CO_2).

3.3 Effect of discontinuity between the plugs in composite cores

SS drainage experiments were performed on a composite core. The composite core (with porosity ϕ=0.20 and length, L=15.69cm) is made using two plugs with permeabilities 1903 mD and 893 mD for the first and last part of the composite core, respectively. The results for this composite core were simulated using single component phases with equilibrium properties (immiscible system). The significant drop in Sw observed at contact between the two plugs (see Figure 5) was investigated by additional simulations. Three simulations were run with the following assumptions:

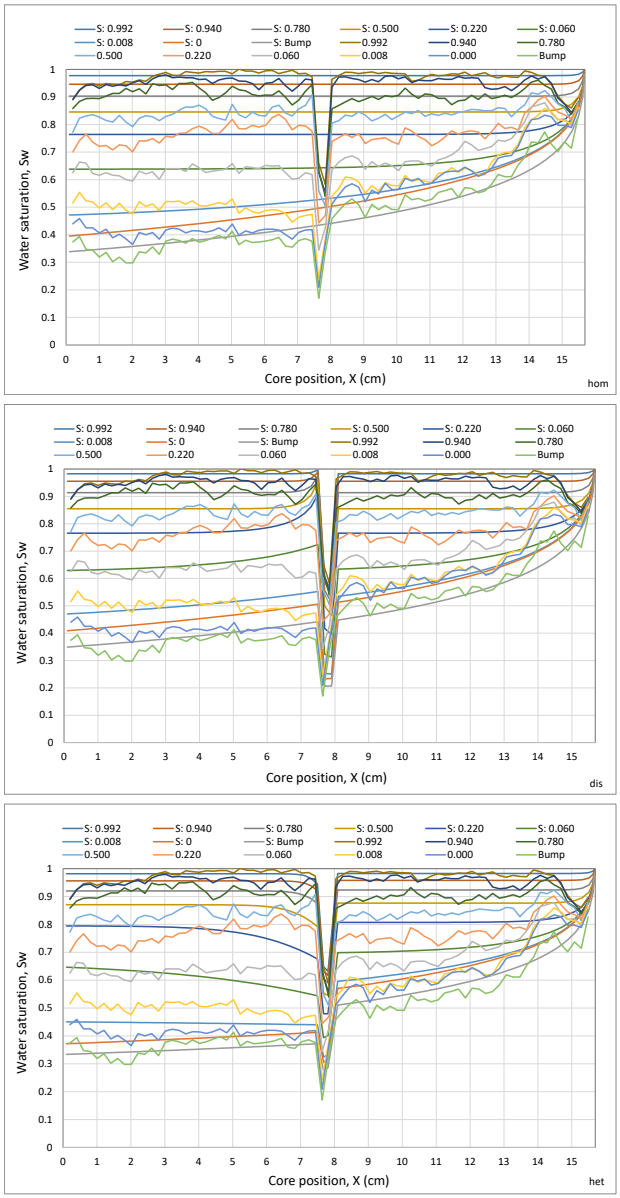

Figure 5 Simulated and experimental saturation profiles. Fractional flow of water is indicated in the legend and S: and fw: indicates simulated and experimental data, respectively. Top: homogeneous core, middle: homogeneous core with discontinuity, bottom: heterogeneous core with discontinuity.

Homogeneous core – It is assumed same average permeability (1166 mD) for the two plugs and no saturation drop due to plugs' barrier.

Homogeneous core with a discontinuity at contact – It is assumed same average permeability (1166 mD) for the two plugs, but the saturation drop due to plugs' barrier is accounted for in the simulations.

Heterogeneous core with a discontinuity at contact – different plug permeabilities for the two plugs are used and the saturation drop due to plugs' barrier is accounted for in the simulation. for allocation of the permeabilities to the plugs, measured plug permeability at ambient conditions were scaled to the composite core permeability measured at reservoir conditions. The scaled plug permeabilities were assigned to the first and last part of the composite core, respectively.

According to Figure *6*, the estimated relative permeability functions are similar for the three cases. For water, k_{rw} is slightly higher for the homogeneous case with discontinuity. For the gas phase, k_{rg} is the same at low gas saturations, but higher for the heterogeneous case at higher gas saturation. Only small differences can be seen in the capillary pressure with the heterogeneous case slightly below the other cases at higher water saturation.

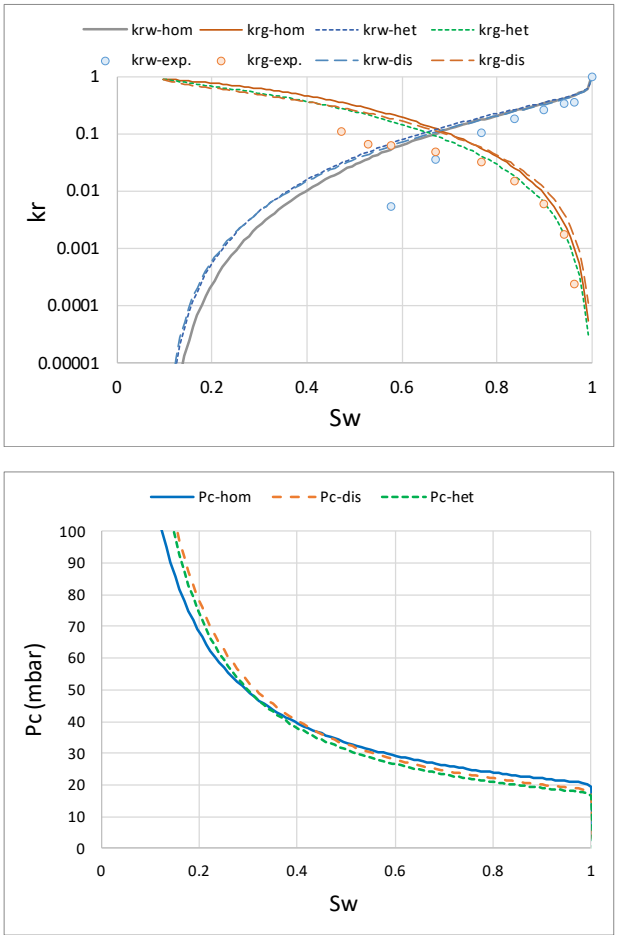

Figure 6 Capillary pressure history matched, three cases: hom.: Homogeneous core, dis.: Homogeneous core with a discontinuity at contact, het.: Heterogeneous core with a discontinuity at contact.

3.4 Measured vs. simulated capillary pressure

Instead of incorporating capillary pressure directly into the history matching (HM) process, measurements obtained from Mercury Injection Capillary Pressure (MICP) tests were used. These results were then compared with a scenario in which both relative permeability and capillary pressure were treated as tuneable parameters in the HM. Figure 7 to Figure 9 illustrate this comparison, clearly demonstrating a better match when capillary pressure was included in the history matching process. This suggests that the capillary pressure between water and CO_2 under reservoir or supercritical conditions differs from capillary pressure measurements conducted at ambient conditions (MICP method); a conclusion also supported by Ebeltoft et al [4] for ambient multispeed Pc measurements.

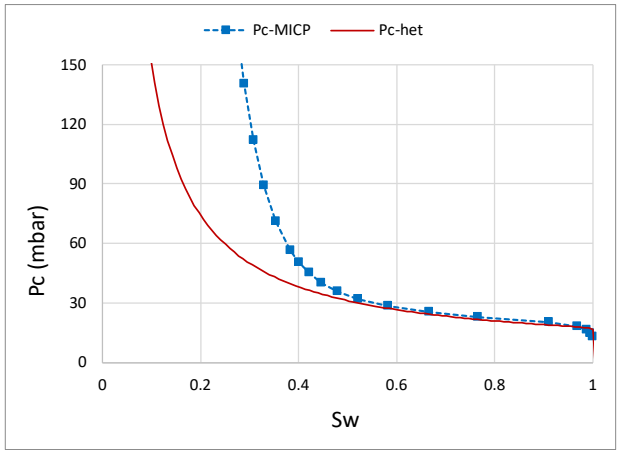

Figure 7 History matched vs. measured (MICP) capillary pressure curves.

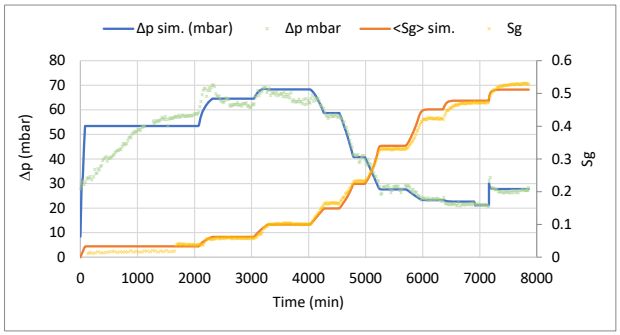

Figure 8 Match using the measured MICP data.

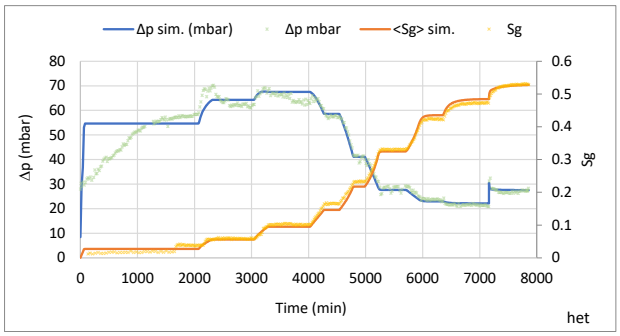

Figure 9 Match by including the capillary pressure in the HM.

3.5 Reliability of relative permeabilities at low S_{ws}

Due to strong capillary end-effects in SS drainage process and that the viscous force cannot overcome the capillary forces to achieve k_r-S_w data at low water saturations (typically lower than 50-60%) the estimated relative permeability and capillary pressure curves in this region are not of high reliability.

A sensitivity HM series was performed by varying S_{wir} and K_{rg}. Results show that the overall match of Δp and Sg is good and similar for all cases. In addition, in the experimentally observed saturation range (i.e., S_w>0.6), the estimated relative permeability functions for water and CO_2 are remarkably consistent across all cases. However, at water saturations below 0.6, relative permeabilities, especially that of CO_2, exhibit significantly different trends. Notably, while all these scenarios produce rather consistent matches for both the Δp and S_g they reveal substantial variability in the relative permeability behaviour at lower water saturations, i.e. beyond the experimental saturation coverage.

This outcome highlights the limited sensitivity of history matching differential pressure and saturation profiles to the specified values of irreducible water saturation (S_{wir}) and the corresponding gas relative permeability (k_{rg}) within the experimentally covered saturation range. However, beyond this range, the estimation of relative permeabilities becomes highly sensitive to these parameters. This underscores the importance of accurately measuring S_{wir} and k_{rg} under realistic reservoir conditions—namely, representative temperature, pressure, and fluid equilibrium—to ensure reliable extrapolation and model predictions.

4. SCAL-model workflow

To prepare data for the dynamic model, we applied a two-step SCAL procedure that makes the uncertainty explicit. *Step 1 – endpoint correlations.* Irreducible water saturation is correlated to water permeability (S_{wir} versus kw) and trapped gas saturation is correlated to initial water saturation (S_{gt} versus S_{wi}) using the Land equation. No relative permeability or capillary pressure curves are generated until these anchor points are fixed. *Step 2 – curve construction and uncertainty bounds.* With the end points in place, we draw a base set of k_r–S_w and Pc–S_w tables for both primary drainage and imbibition. An optimistic set (high k_{rw}, low k_{rCO_2}, low Pc) and a pessimistic set (low k_{rw}, high k_{rCO_2}, high Pc) are then added so that the three families bracket all analogue data.

All tables are first normalised to 0–1 saturation and later rescaled in each grid block with the local S_{wir}–k_w and Land based S_{wi} values. This approach keeps the curve shapes governed by core physics while carrying the full uncertainty range into field scale CO_2 plume and trapping simulations.

4.1 Irreducible water saturation vs. water permeability

Figure 10 plots irreducible water saturation against water permeability for the full analogue dataset and overlays three log-linear regressions that define the SCAL model's uncertainty bounds. The solid black line is the best-fit trend and serves as the base case. The dashed line passes through the lowest S_{wr} values and represents the optimistic scenario—minimal irreducible water, high CO_2 plume mobility and maximal storage capacity—whereas the dotted line honours the highest S_{wr} points and constitutes the pessimistic case, i.e. greatest capillary resistance.

Across almost three decades of permeability (≈ 2 mD to 2 D) the inverse Swir–k relationship is clear: irreducible water declines from ~0.23 at 10 mD to < 0.08 above 1 D. steady-state CO_2/brine measurements and the Hg/air MICP data (converted to CO_2/brine at Pc = 5 bar) cluster tightly, validating the scaling procedure and providing the primary anchor for the regression. Ambient condition N_2 floods plot systematically above the CO_2 points, reflecting the higher interfacial tension of the N_2/brine system, yet remain within the overall envelope. Centrifuge and porous plate results fall in line with these trends, confirming cross method consistency. These three S_{wr}–k correlations are applied grid cell by grid cell in the dynamic model, propagating pore scale uncertainty through both primary drainage and long-term imbibition forecasts for the Poseidon CO_2 storage.

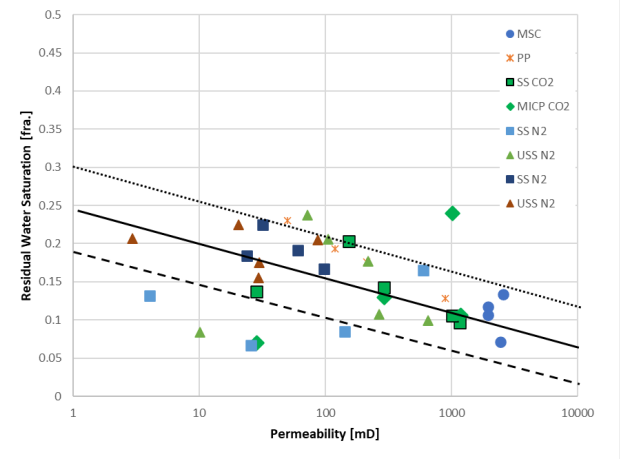

Figure 10 Irreducible water saturation versus permeability for all the samples that has been used in the analogue study

4.2 Trapped saturations vs, initial saturation correlation

The trapped gas saturations determined after primary drainage to irreducible water saturation (S_{wir}) using the porous plate method are shown in Figure 11. The new Analogue-Reservoir dataset (green markers) aligns remarkably well with both the Northern Lights $scCO_2$ results [4] (red markers) and the extensive N_2 benchmark suite (black-outlined symbols) when plotted as residual (trapped) CO_2 saturation versus initial water saturation. Despite differences in fluid ($scCO_2$ vs. N_2), test protocol

(steady-state vs. unsteady-state), and core cleaning, all data fall within the same Lands-type envelope described by the **Lands correlation**:

$$S_{gr}^{*} = \frac{S_{gi}^{*}}{1+CS_{gi}^{*}} \qquad (6)$$

Where S_{gi}^{*} and S_{rg}^{*} are the effective gas saturation, normalized by the irreducible water saturation, and C is the Lands Constand, a rock-dependent empirical parameter that controls the degree of gas trapping during water imbibition.

In our case, the data are bounded by Lands constant of C = 1.5 (lower bound), 2.3 (central curve) and 3.8 (upper bound). In particular, the Analogue-Reservoir points cluster near the mid-range (C≈2.3–2.5), while the N_2 datasets on strongly water-wet cleaned cores tightly bracket Sgr≈0.28–0.38 at Swi≈0.15–0.25, confirming that wettability and flooding method exert only second-order effects on trapping behaviour once proper scaling is applied. These observations validate our "multiple-analogue" strategy: by anchoring on high-fidelity $scCO_2$ core floods (Ivar Aasen, Northern Lights) and bracketing with water-wet N_2 analogues, we can confidently adopt a unified Lands Constant of 2.3 (with a conservative uncertainty range of 1.5–3.8) to represent Swi–S_{gr} for the Poseidon Gassum/Skagerrak sandstones at reservoir conditions. This single, defensible saturation function—complete with quantified bounds—provides robust input for reservoir simulation and risk-informed decision-making in the absence of direct Poseidon core data.

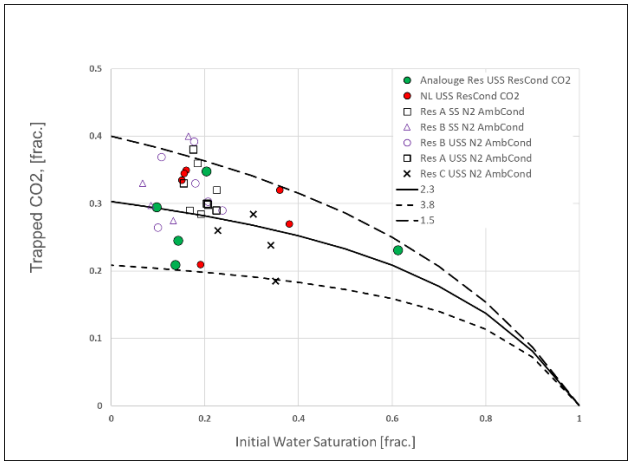

Figure 11 Trapped gaseous phase (N_2 and CO_2) vs, initial water saturation with applied Land correlations.

4.3 Primary drainage, relative permeability and capillary pressure

Figure 12 and Figure 13 present the full ensemble of steady-state CO_2-drainage k_r–S_w measurements (individual core floods shown in black and gray) alongside our three-tier SCAL model, which is anchored on the combined dataset. In both the linear-scale plot Figure 12 and the semilog-scale plot Figure 13 , the solid red curve denotes the base-case LET fit, while the green and blue curves define the pessimistic and optimistic bounds, respectively, chosen to envelope the scatter in the experimental data.

The optimistic bound corresponds to scenarios where k_{rCO_2} is minimized and k_{rw} is maximized—conditions that slow plume advance and maximize storage capacity—whereas the pessimistic bound captures the highest k_{rCO_2} and lowest k_{rw}, implying faster migration and reduced residual trapping. By fitting these three curves to the combined steady-state relative-permeability cloud, we ensure that our SCAL model faithfully represents both the central tendency and the full uncertainty range of CO_2 flooding behavior in our analogue sands.

As evident in Figure 12 and Figure 13, the CO_2 relative-permeability curves display markedly greater scatter near the irreducible-water saturation (S_{wir}) than their water-phase counterparts. This stems from the higher uncertainty in S_{wir} determination during our history-matched, steady-state core-floods—where capillary-end effects induce a non-uniform saturation gradient from inlet to outlet. Because CO_2 connectivity is especially sensitive to these pore-scale saturation variations, k_{rCO_2} near S_{wir} shows larger spread. Although our automated history-matching workflow corrects for the bulk of the end-effect bias, its inversion is inherently less sensitive to subtle shifts in S_{wir}, leaving residual uncertainty in the low-S_w tail of the CO_2 relative-permeability curves.

Figure 14 gathers every drainage Pc measurement used in the study. Three clear trends appear. First, permeability control: plugs with low permeability (≈ 30 mD) exhibit the highest capillary pressures; plugs around 300 mD fall in the mid-range, while 1 D plugs plot lowest. This confirms the expected inverse relationship between capillary pressure and permeability (Pc–k).

Second, method agreement: ambient-pressure N_2 data from two analogue fields—multi-speed centrifuge data (MSC, filled circles) from Reservoir Analogue A and porous plate data (PP, open symbols) from Analogue B show good internal consistency and plot closely to reservoir-condition Hg-air MICP curves. These MICP curves were measured on end caps from the Ivar Aasen cores, which were also used in the $scCO_2$ core flood experiments. After Swanson scaling, the MICP curves align reasonably well with the history-matched Pc curves from the $scCO_2$ floods (blue dashed lines), confirming that ambient Hg-air MICP data can be reliably transferred to the CO_2/brine system under appropriate scaling.

Third, model envelope: the red line represents the base case Pc model, anchored to the Northern Lights porous plate, centrifuge, and scaled MICP data obtained on reservoir cores [4]. Although not acquired at full reservoir pressure and temperature, these data are based on history-matched experiments performed under near-reservoir conditions and are therefore considered more representative of Poseidon than the ambient N_2 analogues. The analogue N_2 data—converted to reservoir conditions—define the upper-bound (pessimistic) curve (green), while the blue curve, which tracks the lowest Pc trend, defines the optimistic limit.

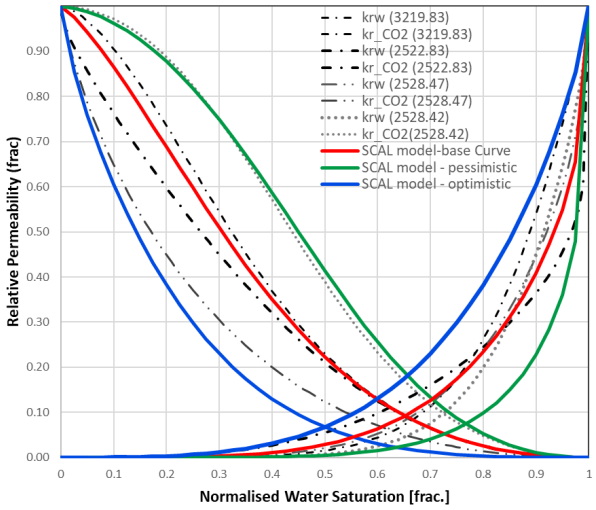

Figure 12 Relative permeability for SCAL-model together with individual interpretation of steady-state scCO2/brine experiments on Ivar Aasen, lin-lin plot. Primary drainage.

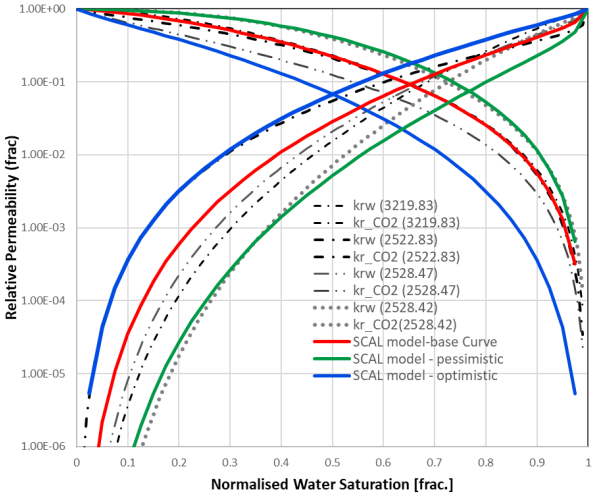

Figure 13 Relative permeability for SCAL-model together with individual interpretation of steady-state scCO2/brine experiments on Ivar Aasen, semilog plot. Primary drainage.

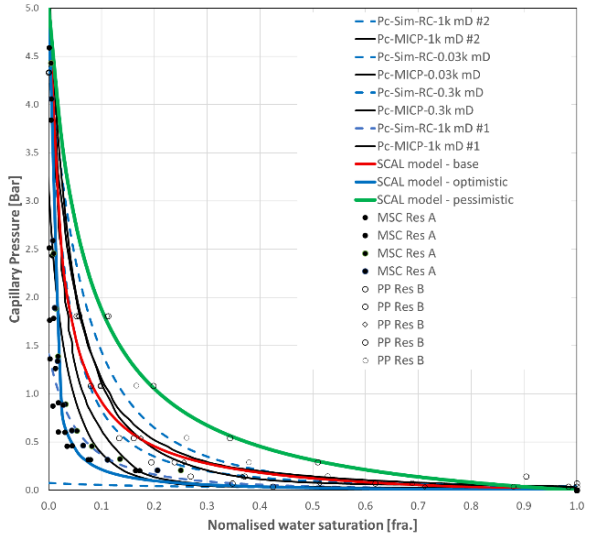

Figure 14 Capillary pressure for SCAL-model that comprises all individual capillary pressure curves. Primary drainage.

The strong agreement across sources—the analogue N_2 datasets, the scaled Hg-air MICP data, and the simulated Pc curves from the Ivar Aasen cores (a Poseidon analogue)—demonstrates consistent behavior across methods, permeability ranges, and fluid systems. Notably, these datasets all fit well within the Pc model envelope defined by [4] for the Northern Lights reservoir, further validating the use of this model for the Poseidon Gassum/Skagerrak sandstones. Together with their matching LET k_r sets, these three Pc curves bracket all observations and provide the necessary input for uncertainty-aware reservoir simulation.

4.4 Imbibition, relative permeability and trapped CO2

Figure 15 gathers all imbibition measurements: ambient N_2/brine floods on cleaned, strongly water-wet plugs and $scCO_2$/brine floods run at reservoir P-T on the same analogue rock. The curves are plotted with the three-level SCAL model. This combined plot forms the reference for setting imbibition parameters in the model. A clear fluid effect appears.

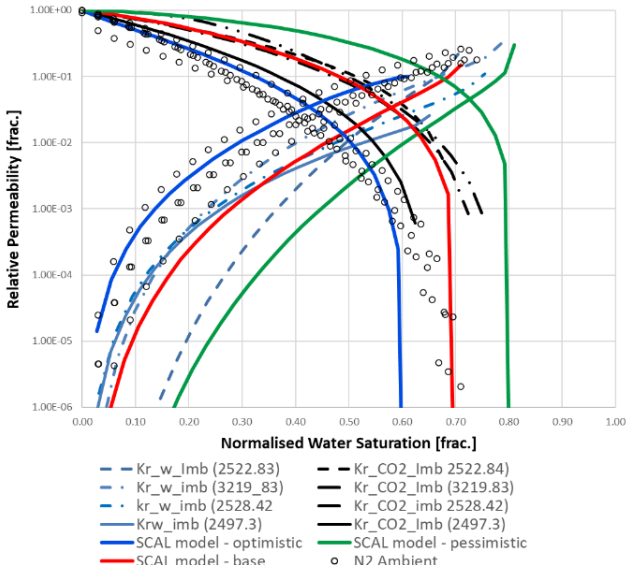

Figure 15 Relative permeability for SCAL-model together with individual interpretation, semilog plot. Imbibition.

At any normalised S_w the N_2 floods give higher k_{rw} than the $scCO_2$ floods. The high N_2–brine interfacial tension keeps brine films connected and allows film flow. By contrast, trapped $scCO_2$ ganglia and the lower CO_2–brine IFT, block water paths and push k_{rw} down, so the water branch shows greater spread. The gas branch behaves the other way: during imbibition k_{rCO_2} from $scCO_2$ tests sits above the N_2 values because the super-critical phase, with lower viscosity and IFT, reconnects easier after snap-off.

These systematic gaps are captured in the SCAL set:

- The **base line** (red) runs through the middle of the $scCO_2$ data;
- The **optimistic line** (blue) pairs low k_{rCO_2} with high k_{rw}, giving maximum trapped gas and the safest storage case;

- The **pessimistic line** (green) has high k_{rCO_2} and low k_{rw}, giving the fastest potential plume rise.

Imbibition curves used in flow simulation are defined in two complementary ways. First, we provide explicit relative permeability (k_r) and capillary pressure (Pc) tables for both primary drainage and imbibition, based on laboratory measurements and bounded by the analogue-based uncertainty envelope. Second, we apply the Killough hysteresis model, which enables the simulator to interpolate between drainage and imbibition curves during saturation reversals, based on local saturation history. Grid cell-specific values for irreducible water saturation (S_{wr}) and Land-based trapped gas saturation (S_{gt}) are used to anchor the hysteresis response in each cell. This dual approach ensures that both the directional fluid behavior and the experimental uncertainty observed in the laboratory are carried into the dynamic model, allowing it to reproduce the range of plausible outcomes during CO_2 injection, migration, and trapping under reservoir conditions.

5 Discussion and Outlook

The analogue SCAL package gives Poseidon its first coherent set of kr-Pc curves and end-point relations, yet several additional steps are required to move from appraisal quality to a development-grade description.

Primary-drainage floods on Poseidon cores. The soon-to-be-drilled appraisal well will recover plugs from both the Gassum and Skagerrak units. Repeating the *primary-drainage* tests with **super-critical CO_2 at full reservoir pressure and temperature** on these plugs is the single most valuable next experiment. Our present drainage data, drawn from Ivar Aasen and other analogues, show S_{wir} ranging from 0.15 to 0.30 and a two-order-of-magnitude spread in k_{rCO_2} near S_{wir}. High-quality P–T representative floods on Poseidon rock will either confirm the current base line or require it to be shifted. Any change in S_{wir} will feed directly into the ultimate capacity estimate; a lower S_{wir} raises the usable pore volume, while a higher S_{wir} reduces it.

Multi-cycle hysteresis. Field operations rarely follow a single drainage–imbibition cycle. Shut-ins, pressure-relief periods and possible brine-withdrawal stages introduce extra scanning paths not captured by first-cycle Killough parameters. Second- and third-cycle SS/USS floods—first on the analogue plugs, later on Poseidon cores—are needed to map those curves and give the model realistic hysteresis behaviour.

Gas-stream purity. Injection gas will carry N_2, O_2 and trace SOx/NOx. Impurity floods under Poseidon P–T will quantify how these species alter interfacial tension, wettability and, by extension, the optimistic, base and pessimistic k_r-Pc envelopes.

Long-term geochemical evolution. Short-duration floods and quick reactive-transport runs suggest only minor calcite dissolution in Poseidon brine, but century-scale storage could still see porosity change from slower feldspar dissolution or clay growth. Coupling the calibrated k_r-Pc sets to a kinetic geochemical model will provide the long-range view needed for injectivity forecasts and seal assessment.

Digital-rock validation. Micro-CT imaging and pore-network modelling on the new Poseidon plugs will supply pore-scale k_r and trapped-gas predictions, giving an independent check on the continuum-scale LET fits derived here.

Probabilistic field forecasting. Embedding the three k_r-Pc families in an ensemble of geological realisations and injection schedules will convert deterministic curves into probability bands for plume extent, pressure build-up and storage efficiency—outputs now expected in risk-based regulatory submissions.

All new core-flood data, Pc measurements, history-match files and uncertainty descriptors will be uploaded to the digital SCAL repository proposed by Petersen et al. (2023), ensuring transparency and shortening lead times for future CCS projects.

6 Conclusions

- **Analogue transfer validated.** After pressure–temperature–IFT scaling, steady-state $scCO_2$ floods on Ivar Aasen plugs, converted Hg-air MICP data and ambient-condition N_2 floods converge within a single Land envelope, confirming that rigorously corrected analogues can stand in for missing Poseidon cores at the appraisal stage.
- **Key endpoint trends established.** Irreducible water- saturation declines loglinearly from ~0.23 at 10 mD to < 0.08 above 1 D, while -trapped gas saturation follows a Land relation with exponent 2.5 ± 1.3. These correlations allow automatic -per cell- scaling of S_{wir} and S_{gt} in the reservoir grid.
- **Three coupled k_r–Pc families delivered.** LET fits generate optimistic, base and pessimistic drainage/imbibition tables that bracket every measured k_r and Pc curve while preserving the observed k_{rw}–k_{rg} trade-off. The optimistic case gives the lowest Pc and highest k_{rw}, maximising residual trapping; the pessimistic case provides the opposite bound.
- **Minor geochemical impact on core-flood timescales.** Reactive-transport calculations show that, at Poseidon brine composition, calcite dissolution alters Ca^{2+}, pH, viscosity and CO_2 solubility only marginally during laboratory floods; hence geochemistry can be omitted from history matching and incorporated later for long-term predictions.
- **Sensitivity concentrated outside the measured S_w range.** Within the experimental saturation window, history matches are insensitive to the choice of S_{wir} and $k_{rg}(S_{wir})$; otherwise, predictions depend strongly on reliable endpoint measurements, underlining the need to obtain these anchors on Poseidon cores.

- **Immediate field impact and wider application.** The analogue based SCAL package—complete with quantified uncertainty bounds—has been implemented in the Poseidon dynamic model, providing the first probabilistic forecast of storage capacity, plume geometry and pressure evolution. The workflow and datasets are being uploaded to the new digital SCAL archive, offering a ready template for other CCS projects that must rely on analogue material in early phases.

Acknowledgement

We would like to extend our gratitude to Aker BP and its license partners on the Ivar Asen and Poseidon fields for granting permission to publish the data and results from this study. Their support has been invaluable in advancing our research.

We also wish to acknowledge NORCE for their contributions through the SCAL laboratory and the interpretation work using IORCoreSim. Their expertise and resources have been crucial in the successful completion of this study.

References

1. Bachu, S. (2008). CO_2 storage in geological media: Role, means, status and barriers to deployment. Progress in Energy and Combustion Science, 34(2), 254–273.
2. Matter, J. M., & Kelemen, P. B. (2009). Permanent storage of carbon dioxide in geological reservoirs by mineral carbonation. Nature Geoscience, 2(12), 837–841.
3. IPCC Special Report on Carbon Dioxide Capture and Storage (2005). Chapter 5: Underground geological storage.
   Bentham, M., et al. (2014). CO_2 storage potential in Europe (CO_2StoP): Final report.
4. Ebeltoft, Einar, Marion Recordon, Renata Meneguolo, Jørgen Gausdal Jacobsen, Reza Askarinezhad, and Richy Pitman. "Special Core Analysis Model–SCAL Model for CCS: Insights from the First Commercial CO2 Project on the Norwegian Continental Shelf, Northern Lights." Petrophysics-The SPWLA Journal 66, no. 01 (2025): 10-25.
5. Petersen, Egil Boye, Alex Larsen, Lee Craig, Erlend Øian, Thomas Schøyen, Alif Be, and Erik Zakariassen. "Rock and Fluid Data: An Integrated Effort on Improving Subsurface Analysis and Modelling Workflows." In SPE Norway Subsurface Conference, p. D011S003R003. SPE, 2022.
6. Lomeland, F., and Ebeltoft, E., 2008, A New Versatile Capillary Pressure Correlation, Paper SCA2008-08 presented at the International Symposium of the Society of Core Analysts, Abu Dhabi, UAE, 29 October–2 November. URL:
7. Lomeland, F., Ebeltoft, E., and Thomas, W.H., 2005, A New Versatile Relative Permeability Correlation, Paper SCA2005-32 presented at the International Symposium of the Society of Core Analysts, Toronto, Canada, 21–25 August.
8. Helland, J. O., and S. M. Skjaeveland. "Relationship between capillary pressure, saturation, and interfacial area from a model of mixed-wet triangular tubes." Water Resources Research 43, no. 12 (2007).
9. Duan, Z. and Sun, R., "An improved model calculating CO2 solubility in pure water and aqueous NaCl solutions from 273 to 533 K and from 0 to 2000 bar," Chemical Geology, vol. 193 (3), pp. 257-271, 2003.
10. Duan, Z., Sun, R., Zhu, C., and Chou, I.-M., "An improved model for the calculation of CO2 solubility in aqueous solutions containing Na+, K+, Ca2+, Mg2+, Cl- and SO42+," Marine Chemstry, vol. 98, pp. 131-139, 2006.
11. CRC Handbook of Chemistry and Physics, 63rd ed. Boca Raton, Florida: CRC Press, Inc., 1982-1983.
12. Land, C.S., 1971, Comparison of Calculated with Experimental Imbibition Relative Permeability, Paper SPE-3360, Society of Petroleum Engineers Journal, 11(4), 419–425. DOI:10.2118/3360-PA